J. Fluid Mech. (1966), *vol.* 26, *part* 3, *pp.* 459–479
Printed in Great Britain

Thermal equilibration behind an ionizing shock

By H. WONG† AND D. BERSHADER
Department of Aeronautics and Astronautics, Stanford University

(Received 4 November 1965 and in revised form 21 February 1966)

The physical mechanisms underlying the relaxation process leading to thermal equilibrium behind ionizing shock waves in argon have been studied through use of optical techniques. The non-equilibrium condition in the relaxation region was investigated experimentally by measuring the shift in the fringes due to a change in the refractive index of the medium with a Mach–Zehnder interferometer. Both electron- and mass-density profiles from the shock front to the equilibrium region were determined. The experimental work has been supplemented by a theoretical analysis of the ionization mechanism to explain the measured profiles and relaxation times.

1. Introduction

The rapid injection of energy into a gas due to shock excitation destroys temporarily the statistical equilibrium among its translational and internal degrees of freedom. Subsequent establishment of equilibrium is a rate process which depends on the collision parameters of the gas. When the characteristic time for this process is longer than that required for shock excitation of the translational modes, there results a time lag in the equipartitional energy exchange, and we find a so-called relaxation zone behind the shock wave. Indeed, we have found in the present studies that there was no measurable ionization immediately behind the shock front, which itself can be considered discontinuous for present purposes; and that the values of gas density, pressure, temperature and velocity corresponded to an increase of random translational energy only. Typical shock front temperatures, for example, were over 50% higher than the equilibrium values.

Proceeding downstream from the shock front, one finds a continuing adjustment of gas conditions in the relaxation zone, leading finally to thermochemical equilibrium. The equilibration takes place by means of multiple and competing processes, including various modes of excitation, de-excitation, ionization, recombination, and elastic collisions between species at different effective temperatures. Physical models to describe the relaxation zone kinetics have been proposed in earlier studies by several investigators, principally Petschek & Byron (1957), Bond (1957), Weymann (1958), and Harwell & Jahn (1964). Quite recently, additional studies have been reported by Brown & Mullaney (1964), and by Morgan (1964). While these works will not be reviewed in any detail, we may note that by now a variety of alternative mechanisms have been proposed,

† Present address: Lockheed Palo Alto Research Laboratory.

some as a result of a purely theoretical analysis, and others based on certain types of experimental data. Of special interest is the work of Harwell & Jahn (1964) who probed the initial part of the relaxation zone by means of microwaves, and were able to establish electron-density distributions in what we term régime I (see § 2) behind shocks of moderate strength. Their results lend support to the two-stage atom–atom inelastic collision mechanism, namely excitation followed by ionization, as the initial ionizing process, since they obtained an activation energy of 11·5 eV corresponding to the first excited state of argon.

In the section which follows, we discuss the model for the mechanism of relaxation. The experimental method is then reviewed; and finally the results are presented together with interpretive comments.

2. Mechanism of ionization behind strong shocks

A starting point for the analysis is: given a shock advancing into a moderately dense, noble gas with sufficient energy to produce thermal excitation, the average energy being in the electron-volt range of one to two, what is the initial electron-producing process? Evidence provided by some of the other investigators mentioned indicates that there is more than one process operating at any one time, and that the initial principal ionization mechanism gives way to another as the dominant process in the latter portion of the relaxation zone. We shall discuss three régimes, referred to by the Roman numerals I, II and III, each characterized by particular dominant reactions. The assumption is made that each species may be described by its own Maxwellian distribution in the relaxation zone. This appears reasonable since average thermal energies are low compared to excitation energies, and the density is relatively high. Thus, a particle will tend to experience a large number of elastic collisions between the inelastic ones which change its internal state. Local translational temperatures of the electrons and of the heavy particles may well be different in view of the well known inefficiency of elastic transfer of energy between particles of considerably different masses. Further, the temperature difference may vary from point to point in the relaxation zone. We now consider the three régimes in more detail.

Régime I

In régime I the most probable ionization processes are atom–atom collisions, atom-impurity collisions, or photo-ionization by ultraviolet absorption. To reduce the probability of impurity influence, a high purity in the test chamber was achieved, resulting in an impurity level less than 10 parts per million. The combined outgassing and leak rate was 6×10^{-6} mmHg/min. On this basis, it was felt that the effect of impurities could be disregarded; a conclusion which was supported by the experimental data of Harwell & Jahn, where it was found that the impurity influence became less as the shock strength was increased.

To assess the influence of photo-ionization, an elementary radiative-transfer analysis was made. Such transfer would be associated primarily with the argon-atom-resonance lines, for which the absorption coefficient would be much larger than for continuum radiation. The radiation is assumed to originate in the

equilibrium zone. In order to affect conditions at the shock front, radiation of wavelength corresponding to 11·5 V or higher energy would have to penetrate the complete relaxation zone. Photons which make such penetration would then be capable of raising ground state atoms just in front of the shock to an excited or ionized state. A conservative model for the radiation, namely a Planckian black body, was chosen, and the resultant degree of photo-ionization at the shock front was found to be 10^{-12} or less. Part of the difficulty in any assessment lies in accounting for additional radiation sources in the relaxation zone. On the basis of the present model, however, it appears that photo-ionization can be ignored.

Turning now to atom–atom collisions, we note first that the atom–atom process may involve two possible mechanisms:

(*a*) a single step process leading to ionization

$$A + A \rightarrow A^+ + e + A,$$

(*b*) a two-step process leading to excitation, then followed by ionization

$$A + A \rightarrow A^* + A,$$
$$A^* + A \rightarrow A^+ + e + A.$$

Weymann (1958) has shown theoretically that the two-step process is more efficient. The theory is based on the fact that the probability for excitation is greater than for ionization of an atom from ground state, and that the probability for ionization of an excited state is more favourable than de-excitation. The excited atoms, having a lifetime of 10^{-8} sec, can be de-excited by spontaneous radiation, by collisions with the wall, or with other atoms. But since argon is optically thick at the wavelength of its resonance radiation (1078 Å) in the density régime corresponding to $N_A = 6 \times 10^{17}\,\mathrm{cm}^{-3}$, the radiation is readily reabsorbed by other atoms. Hence, the ionization from the excited states effectively over-balances the destruction of the excited states. In addition to the theoretical study, there is experimental evidence (Johnston & Kornegay 1963, and Harwell & Jahn 1964) that the two-step ionization process is the dominant process in this régime. Since the probability for subsequent ionization of excited states is several orders of magnitude larger than that for atoms in the ground state, the initial step of the two-step process becomes the rate-controlling one. As a result, there is no net accumulation of atoms in the excited states, and the rate of ionization is essentially equal to the rate of excitation.

Due to the lack of information on the atom–atom ionization cross-section near threshold, the cross-section for this process must be obtained experimentally. In the shock tube, collisions take place under gas-kinetic conditions where multiple collisions are possible, as contrasted with an atomic beam experiment where the flux of incoming particles is of known energy and the particles encounter only single collisions. Under present experimental conditions, only the temperature, and hence the Maxwellian velocity distribution of the gas atoms are known. However, by utilizing the rate equation, one can achieve the functional form of the cross-section by knowing the velocity distribution of the atomic species and the manner in which the electron-density production and neutral-atom density change with temperature. The rate equation for electron

production by argon atom–atom inelastic collisions written in the centre-of-mass system is

$$\frac{dN_e}{dt} \equiv \frac{dN_{A^*}}{dt} = \frac{8}{\pi}\left(\frac{m_A}{2kT}\right)^3 N_A^2 \int_0^\infty v_{cm}^2 \exp\left(-m_A v_{cm}^2/2kT_A\right) dv_{cm} \int_{g_0}^\infty g^3 \sigma_{in}(g) \times \exp\left(-m_A g^2/4kT_A\right) dg, \quad (1)$$

where N_A is the number density of the atoms, N_{A^*} is the number density of atoms in the first excited state, g is the relative speed of the species, $\sigma_{in}(g)$ is the inelastic cross-section, v_{cm} is the velocity of the centre of mass, and g_0 is the velocity corresponding to the first excited state of argon. To reduce the rate equation to a simpler form, define

$$y = (g/g_0)^2 = E/E_0, \quad \theta(y) = \sigma_{in}(y)/\sigma_0, \quad s = \mu g_0^2/2kT_A, \quad \mu = \tfrac{1}{2}m_A,$$

where σ_0 is a reference cross-section. Further, use can be made of the experimentally verified relation (Harwell & Jahn 1964, and Johnston & Kornegay 1963)

$$\frac{dN_e}{dt} = c_2 e^{-s},$$

where c_2 is an experimentally determined coefficient. Next, we note that

$$N_A = p/kT = 4ps/m_A g_0^2.$$

Upon substitution of the above expressions, equation (1) becomes

$$e^{-s} s^{-\frac{7}{2}} = \int_1^\infty y \frac{\theta(y)}{B} e^{-sy}\, dy, \quad (2)$$

where

$$B = \frac{\sqrt{\pi}}{2^{\frac{3}{2}}}\left(\frac{c_2}{g_0\sigma_0}\right)\left(\frac{m_A g_0^2}{4p}\right)^2.$$

Since the degree of ionization is small in this régime, the pressure change is slight and thus p can be assumed constant. The constant quantity B can be evaluated from corresponding values of c_2 and p obtained experimentally. Next, if we let

$$y' = y - 1, \quad f(y) = y\theta(y)/B,$$

equation (2) can be rewritten as

$$s^{-\frac{7}{2}} = \int_0^\infty f(y'+1)\, e^{-sy'}\, dy'.$$

The right-hand side of this equation is just the Laplace transform of $f(y'+1)$, and thus this function is given by

$$f(y'+1) = \frac{1}{2\pi i}\int_{a-i\infty}^{a+i\infty} s^{-\frac{7}{2}} e^{sy'}\, ds,$$

which yields, after replacing y' by $y-1$,

$$f(y) = \frac{8}{15\sqrt{\pi}}(y-1)^{\frac{5}{2}}.$$

Resubstitution then gives the inelastic cross-section as

$$\left.\begin{aligned} \sigma(E) &= \frac{2^{\frac{3}{2}}c_2}{15g_0}\left(\frac{E_0}{p}\right)^2 \frac{(E/E_0-1)^{\frac{5}{2}}}{E/E_0}, \\ \text{or} \qquad \sigma(E) &= \frac{1{\cdot}7 \pm 0{\cdot}3 \times 10^{-18}(E/E_0-1)^{\frac{5}{2}}}{E/E_0}\ \text{cm}^2. \end{aligned}\right\} \tag{3}$$

The manner in which the cross-section is evaluated is discussed in § 5.

If dN_e/dt is written in terms of a rate constant in the usual way,

$$\frac{dN_e}{dt} = N_A^2 K_A(T_A),$$

then the above analysis yields the following results for $K_A(T_A)$

$$K_A(T_A) = 8{\cdot}9 \times 10^{-12}(kT_A/E_0)^2 \exp(-E_0/kT_A)\ \text{cm}^3/\text{sec}. \tag{4}$$

The electrons produced in the above manner have, at first, relatively low energy, since most of the impact energy is utilized as energy of ionization. As their number increases, the average electron energy also begins to increase, as a result of elastic collisions with the more energetic neutral and ionic particles. A second mechanism for ionization then arises, namely electron–atom inelastic collisions, which characterizes régime II.

Régime II

A theoretical approach similar to that of Petschek & Byron (1957) will be followed here. When the number of electrons becomes sufficiently large, these particles begin to serve as effective energy-transfer agents for producing ionization by inelastic impacts with neutrals after having acquired energy through elastic collision with the heavy species. Such ionizing collisions effectively obscure all other processes of ionization because of their relatively large cross-section. At this stage, there is a high enough density of electrons so that these particles will attain a Maxwellian distribution among themselves. The effective electron temperature remains lower than that of the heavy particles since the electrons lose most of their energy upon ionization. To analyse the energy exchange, one needs to compare the energy gained by electrons in superelastic collisions with that lost by inelastic collisions. The exchange of kinetic energy by elastic collisions can take place either with atoms or ions. Before treating either individual case, we formulate the problem more generally. The exchange rate in the centre-of-mass system is

$$\left(\frac{d\epsilon}{dt}\right)_{el} = -N_e N_A \mu \int_0^\infty (\mathbf{v}_{cm}\cdot\mathbf{g})\sigma_{el}(g) g f_e f_A \, d\mathbf{v}_{cm}\, d\mathbf{g}, \tag{5}$$

where μ is the reduced mass, f_e, f_A are Maxwellian distributions for electrons and atoms respectively, and $\sigma_{el}(g)$ is the diffusion-momentum-transfer cross-section. Expanding exponential terms involving quantities $(m_e/2kT_A)(T_A/T_e - 1)$, which is small if T_e is of the order of T_A, we obtain

$$\begin{aligned} \left(\frac{d\epsilon}{dt}\right)_{el} = \left(\frac{m_e^2}{m_A}\right) N_e N_A \left(\frac{T_A}{T_e}-1\right) \Bigg\{ &\int_0^\infty g^3 \sigma_{el}(g) f_e \, d\mathbf{g} \\ &+ N_e N_A \left(\frac{m_e^2}{m_A}\right)^2 \left(\frac{1}{2kT_A}\right) \left(\frac{T_A}{T_e}-1\right)^3 \int_0^\infty g^5 \sigma_{el}(g) f_e \, d\mathbf{g} \Bigg\}. \end{aligned} \tag{6}$$

The exact solution to equation (5) has been given by Boulegue *et al.* (1958). The first term of the solution as given above is just that reported by Petschek & Byron (1957). The second term is a higher-order term in the expansion, and is neglected in what follows.

For the case where the heavy particle is an ion, the diffusion cross-section is determined by the Coulomb cross-section. The resulting equation for energy gain is

$$\left(\frac{d\epsilon}{dt}\right)_{el_1} = \frac{N_e N_{A^+} e^4}{m_A}\left(\frac{T_A}{T_e}-1\right)\sqrt{\left(\frac{8\pi m_e}{kT_e}\right)}\ln\left(\frac{9(kT_e)^3}{4\pi N_e e^6}\right), \tag{7}$$

where the subscript 1 refers to the Coulomb interaction.

For the case where the heavy particle is an atom, the cross-section will involve the Ramsauer effect. If we define (De Voto 1964)

$$Q(T_e) = (m_e/2kT_e)^3 \int_0^\infty \sigma_{el}(g) g^5 \exp(-m_e g^2/2kT_e)\, dg, \tag{8}$$

the energy transferred is

$$\left(\frac{d\epsilon}{dt}\right)_{el_2} = \frac{4}{\sqrt{\pi}} N_e N_A \left(\frac{m_e^2}{m_A}\right)\left(\frac{2kT_e}{m_e}\right)^{\frac{1}{2}}\left(\frac{T_A}{T_e}-1\right) Q(T_e), \tag{9}$$

where the subscript 2 refers to the neutral interaction. The combined energy transferred elastically is given by

$$\left(\frac{d\epsilon}{dt}\right)_{el} = \left(\frac{d\epsilon}{dt}\right)_{el_1}\{1+Z(N_e, T_e, N_A)\}, \tag{10}$$

where

$$Z(N_e, T_e, N_A) = \left(\frac{d\epsilon}{dt}\right)_{el_2}\Big/\left(\frac{d\epsilon}{dt}\right)_{el_1} = 4{\cdot}56\times 10^5 \frac{N_A T_e^2 Q(T_e)}{N_e \ln(1{\cdot}54\times 10^8 T_e^3/N_e)},$$

and where c.g.s. units are to be used for the various physical quantities.

The ionization process in this régime is assumed to be controlled predominantly by the electron collision process: two-step processes (excitation followed by ionization) and single-step processes leading directly to ionization. The three processes involved are:

(1) $A^+ + e \rightarrow A^+ + e$ (elastic),

$A + e \rightarrow A + e$ (elastic),

(2) $A + e \rightarrow A^* + e$,

$A^* + e \rightarrow A^+ + e + e$,

(3) $A + e \rightarrow A^+ + e + e$.

The electron production rate per unit volume is expressed by

$$dN_e/dt = N_e N_A \int f_e u_e \sigma_{in}(u_e)\, d\mathbf{u}_e, \tag{11}$$

where f_e is the electron-velocity-distribution function, u_e the electron velocity and $\sigma_{in}(u_e)$ is the total inelastic cross-section which includes both processes; and

where the atoms are assumed stationary relative to electrons. The total inelastic cross-section obtained by Maier-Leibnitz (1935) is approximated by (figure 1)

$$\left.\begin{aligned} \sigma_{in} &= 7\times10^{18}(E-11{\cdot}5)\,\text{cm}^2 \qquad \text{for} \quad E \leqslant 15{\cdot}75\,\text{eV},\\ \sigma_{in} &= 7\times10^{18}(15{\cdot}75-11{\cdot}5)+2{\cdot}22\times10^{-17}(E-15{\cdot}75)\,\text{cm}^2\\ &\qquad\qquad \text{for} \quad E > 15{\cdot}75\,\text{eV}. \end{aligned}\right\} \tag{12}$$

The explicit expression for the rate then reads as follows:

$$\frac{dN_e}{dt} = 4{\cdot}4\times10^{-6}N_eN_A\left(\frac{(2kT_e)^3}{\pi m_e}\right)^{\frac{1}{2}}\left\{\left(\frac{\beta_E}{T_e}+2\right)e^{-\beta_E/T_e}+\frac{\beta_E}{T_e}\left(1+\frac{\theta_I}{T_e}\right)\left(\frac{\theta_I}{\beta_E}-1\right)e^{-\theta_I/T_e}\right.$$
$$\left.+\,2{\cdot}16\left(\frac{\theta_I}{T_e}+2\right)e^{-\theta_I/T_e}\right\}, \tag{13}$$

where β_E is the excitation temperature, and θ_I is the ionization temperature.

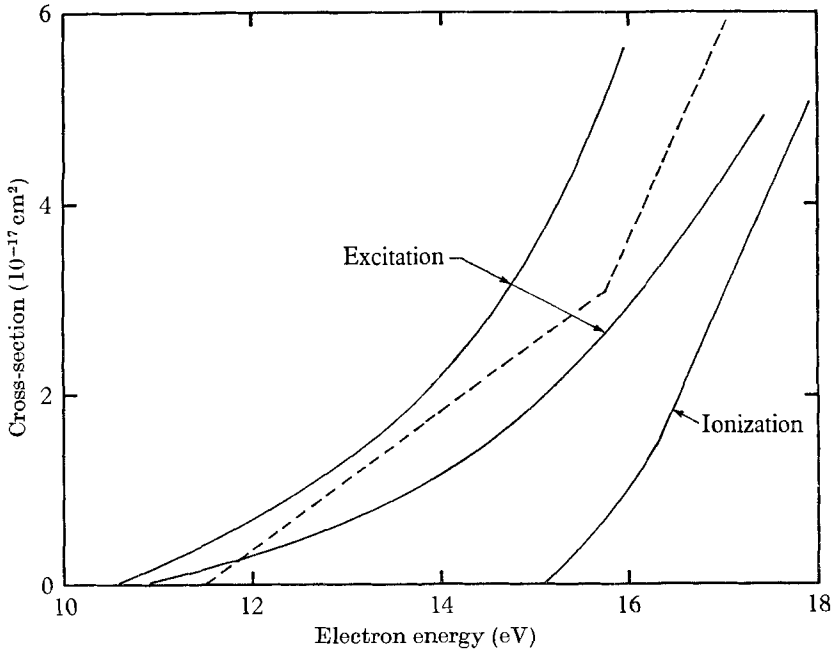

FIGURE 1. Inelastic cross-section for electron–argon atom collisions. ——, Maier-Leibnitz (1935), and Petschek & Byron (1957); – – –, proposed curve for present analysis.

By formulating an energy balance for the electrons we shall obtain a relation between the temperature of the electrons and that of the heavy particles. The electrons can gain energy through elastic collisions with 'hot' ions or atoms, and they can lose energy by ionization, radiation and elastic collisions with other electrons. The assumptions made are:

(*a*) Radiation losses are small.

(*b*) Elastically energized electrons lose energy rapidly in ionization and lose relatively small amounts of energy to other electrons. As a result, the average energy of the electrons does not change appreciably.

(c) Diffusion is negligible because of the high density, large charge-exchange cross-section and no extended gradient near the wall (small boundary layer). The energy loss of the electron gas is written

$$\left(\frac{d\epsilon}{dt}\right)_{in} = (\tfrac{3}{2}kT_e + k\theta_I)\frac{dN_e}{dt}, \tag{14}$$

where $\frac{3}{2}kT_e$ is the thermal energy of the electrons and $k\theta_I$ is the ionization energy. For the energy balance we have

$$\left(\frac{d\epsilon}{dt}\right)_{in} = \left(\frac{d\epsilon}{dt}\right)_{el}. \tag{15}$$

The relation between electron and atom temperatures as a function of the degree of ionization is obtained as

$$\frac{T_A}{T_e} = 1 + \frac{m_A}{e^4}\left(\frac{k^3}{8\pi m_e}\right)^{\frac{1}{2}} \frac{T_e^{\frac{3}{2}}(\frac{3}{2}+\theta_I/T_e)K_I(T_e)}{(1+Z)\ln\{9(kT_e)^3/4\pi N_e e^6\}}\frac{(1-\alpha)}{\alpha}, \tag{16}$$

where
$$K_I(T_e) = 10^{-6}\left\{\frac{(2kT_e)^3}{\pi m_e}\right\}^{\frac{1}{2}}\left\{4{\cdot}4\left(\frac{\beta_E}{T_e}+2\right)e^{-\beta_E/T_e} + 9{\cdot}5\left(\frac{\theta_I}{T_e}+2\right)e^{-\theta_I/T_e}\right.$$
$$\left. + 4{\cdot}4\frac{\beta_E}{T_e}\left(1+\frac{\theta_I}{T_e}\right)\left(\frac{\theta_I}{\beta_E}-1\right)e^{-\theta_I/T_e}\right\} \text{ cm}^3/\text{sec}, \tag{17}$$

and $\alpha = N_e/(N_e+N_A)$ is the degree of ionization.

Régime III

In the early stages of equilibration, the inelastic collision processes are overwhelmingly in the direction of excitation and ionization. As the gas approaches the equilibrium state, recombination processes must be considered as well. Inclusion of these recombination processes in the analysis characterizes régime III.

In recombination of a plasma, there is a general loss mechanism known as collisional-radiative recombination (Bates, Kingston & McWhirter 1962, Byron *et al.* 1962), which is not simply the sum of collisional and radiative recombination but a combination of interacting collisional and radiative processes. The radiative recombination which is predominant in a tenuous plasma and the collisional processes predominant in a dense plasma are two limiting cases of the general loss mechanism. The analysis of electron-atomic-ion recombination by Bates *et al.* (1962) may be applied to argon. In accordance with their model, the upper states tend to equilibrate rapidly with the unbound continuum states, with the result that the net recombination rate (loss of electrons) is equal to the formation of atoms in the ground state by collisional de-activation and spontaneous transitions from excited states, and by three-body and radiative-recombination processes from the continuum. When the plasma is dense, the recombination rate is controlled mainly by collisional transitions from excited states to the ground state.

In the present study, the principal difficulty in evaluating the recombination rate by an appropriate collisional-radiative model is that the cross-sections and transition probabilities of these processes are unknown. However, the approxi-

mate analysis used here will assume only three-body recombination to the ground state; all the excited states, in turn, are assumed to be in equilibrium.

A more general expression for the electron production rate, which applies now to both régimes II and III, is

$$dN_e/dt = N_e N_A K_I(T_e) - N_e^3 K_R(T_e). \tag{18}$$

In turn the relation between electron and atom temperature shows an added term introduced by recombination, in comparison with equation (16)

$$\frac{T_A}{T_e} = 1 + \frac{m_A}{e^4}\left(\frac{k^3}{8\pi m_e}\right)^{\frac{1}{2}} \frac{T_e^{\frac{3}{2}}(\frac{3}{2} + \theta_I/T_e)\, K_I(T_e)}{(1+Z)\ln\{9(kT_e)^3/4\pi N_e e^6\}}\{(1-\alpha)/\alpha - N_e/K_E(T_e)\}, \tag{19}$$

where $K_E(T)$ the equilibrium constant is given by

$$K_E(T) = \frac{12(2\pi m_e)^{\frac{3}{2}}}{h^3}(kT)^{\frac{3}{2}}\exp(-\theta_I/T). \tag{20}$$

Relaxation

Combining régimes I, II, and III and taking all processes into account, we obtain the net rate of electron production

$$dN_e/dt = N_A^2 K_A(T_A) + N_e N_A K_I(T_e) - N_e^3 K_R(T_e). \tag{21}$$

Our considerations so far have applied to some reacting gas in a 'box' so to speak, which gives the change of electron content in a unit volume of shock-heated fluid as a result of chemical change only, and does not account for gasdynamic changes of fluid density. At this time therefore, the mass density may be taken as constant, and we may write

$$\frac{dN_e}{dt} = \frac{\rho}{m_A}\frac{d\alpha}{dt}. \tag{22}$$

Equation (21) becomes

$$d\alpha/dt = (1-\alpha)N_A K_A(T_A) + N_e(1-\alpha)K_I(T_e) - \alpha N_e^2 K_R(T_e). \tag{23}$$

Now, however, the 'reacting-gas-in-a-box' treatment must be made compatible with the fact that the gas is in motion through the flow field. This is accomplished by introduction of the conservation and state equations. In this connexion, it should be mentioned that we are using a two-temperature equation of state

$$p = \rho(k/m_A)(T_A + \alpha T_e). \tag{24}$$

For a given set of initial conditions, the electron and mass densities may be obtained by integrating the rate equation under the constraints of these relations. For this purpose, the latter may be manipulated to yield the following expression between T_A and T_e

$$T_A + \alpha T_e = \alpha T_1 M^2\left(\frac{4 + p/p_1 - 2\alpha\theta_I/T_1}{1 + 4p/p_1}\right)\left(\frac{3(p/p_1 - 1) + 2\alpha\theta_I/T_1}{1+4p/p_1} + \frac{1}{\gamma M^2}\right), \tag{25}$$

where the pressure ratio is

$$\frac{p}{p_1} = \tfrac{1}{8}[3 + 5M^2 + 5\{(M^2-1)^2 + \tfrac{32}{12}\alpha M^2\theta_I/T_1\}^{\frac{1}{2}}].$$

Our problem, then, is to seek simultaneous solutions of equations (19) and (25) before integrating equation (23). We illustrate a graphical procedure in figure 2, a plot of T_A against T_e with α as a parameter. The figure shows two families of

curves, one resulting from chemical-kinetic considerations (equation (19)), the other from gasdynamic laws (equation (25)). The points formed by the intersections of pairs of curves from the two families having the same value of α, determine a curve in the $T_A - T_e$ space which gives the real history of the atom and electron temperatures through the relaxation zone.

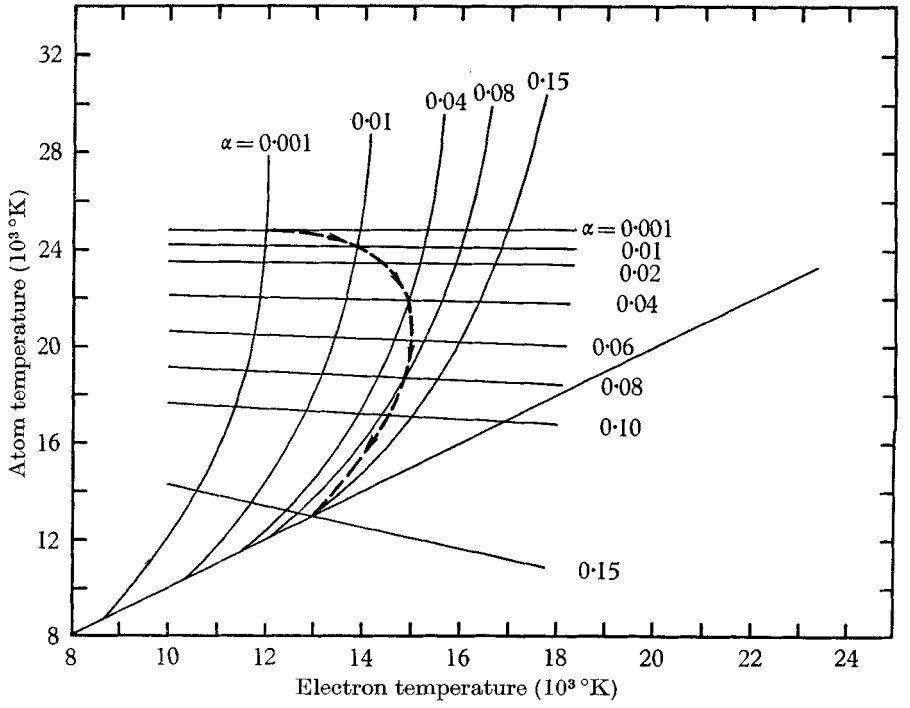

FIGURE 2. Atom and electron temperature in relaxation region for $M = 16{\cdot}3$, $p_1 = 0{\cdot}5$ cm. ---, Particle path through the relaxation region.

It is desirable to integrate the rate equation in a co-ordinate system moving with the shock (see figure 3), for then the phenomena may be described by steady-state relations. Thus,

$$\frac{d\alpha}{dt} = u\frac{d\alpha}{dx''}, \tag{26}$$

where dx'' represents the distance moved by a fluid element relative to the shock front during dt, and where u is its relative velocity. The equation is derived in the laboratory system of co-ordinates, since the system is of prime importance for interpretation of experimental results. One may solve for x'' corresponding to any particular value of α. In particular, for the total extent of the relaxation zone x''_{eq}, one has

$$x''_{\mathrm{eq}} = \int_0^{\alpha_{\mathrm{eq}}} \frac{u\,d\alpha}{(1-\alpha)N_A K_A(T_A) + N_e(1-\alpha)K_I(T_e)\{1-\alpha N_e/(1-\alpha)K_I(T_e)\}}, \tag{27}$$

where

$$u = u_1 - u_2 = a_1 M \frac{4 + p/p_1 - 2\alpha\theta_I/T_e}{1 + 4p/p_1}.$$

The temperature and density profiles are obtained by solving the above equations on a computer.

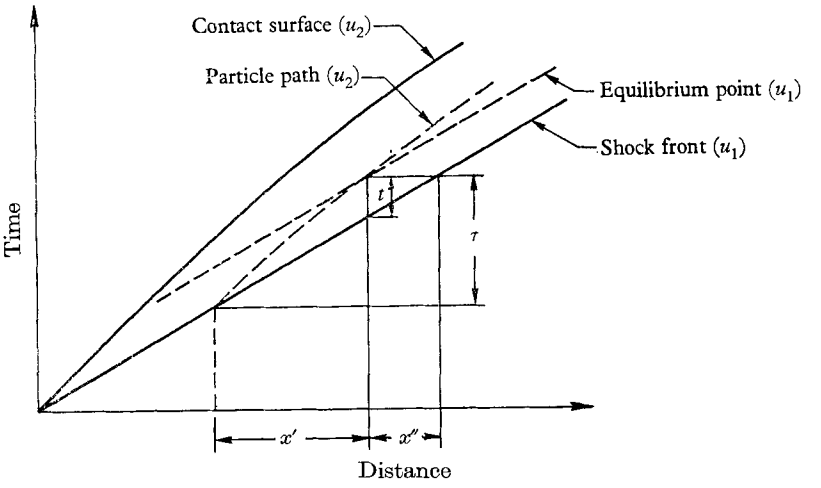

FIGURE 3. (x,t)-diagram of shock tube flow.

Time-scale conversion

The time t measured on the film is in the laboratory time scale. The time of interest is from the instant the shock sets the fluid particles into motion to the point where equilibrium conditions are reached. From figure 3, let x'' be the relaxation distance to the shock front in the laboratory system, t the relaxation time in the laboratory distance system, x' the total particle relaxation distance, τ the total particle relaxation time. The relation between the measured laboratory time to the particle time is given by

$$\tau = (\rho_2/\rho_1)t \quad \text{and} \quad t = (x''/u_1).$$

These relations will be valid for instances where the density ratio ρ_2/ρ_1 (hence $u_1 - u_2$) does not change with time as is the case at zero ionization. However, for large degrees of ionization the density behind the shock varies with time. As a result the time conversion is given by

$$\tau = \int (\rho/\rho_1)\, dt,$$

where the density profile must be known.

3. Interferometry

A dielectric material, in the presence of an applied electric field **E** such as that associated with a travelling light wave, will develop a polarization field **P**, defined as the induced dipole moment per unit volume. The latter is ordinarily proportional to the applied field **E**, with the constant of proportionality termed the polarizability ξ. It is the polarizability of the material which will, in accordance with electromagnetic theory, determine its refractive behaviour. For a dilute medium containing different species, the polarization is taken to be

$$\mathbf{P} = \sum_i N_i \xi_i \mathbf{E},$$

where N_i is the number density of species i, with polarizability ξ_i. The relationship between the refractive index, dielectric constant, and the polarizability can be readily obtained from the constitutive equations of Maxwell and equation of motion for the charged particles. The phase index n can be written as

$$n^2 = \tfrac{1}{2}K_e + \tfrac{1}{2}\sqrt{\{(K_e)^2 + (4\pi\sigma/\omega)^2\}}, \tag{28}$$

where K_e and σ are the real dielectric constant and conductivity respectively, and ω is the impressed frequency.

The various currents in the medium are:

$$\left.\begin{aligned}
&(a)\ \text{electron current} \\
&\qquad \mathbf{j}_e = N_e q\mathbf{u} = \frac{N_e q^2 \mathbf{E}}{m_e}\frac{\nu_c + i\omega}{\omega^2 + \nu_c^2}, \\
&(b)\ \text{ion-polarization current} \\
&\qquad \mathbf{j}_l = \xi_l N_l \frac{\partial \mathbf{E}}{\partial t}, \\
&(c)\ \text{polarization current of the neutral atoms} \\
&\qquad \mathbf{j}_n = \frac{\partial \mathbf{P}}{\partial t} = \xi N_n \frac{\partial \mathbf{E}}{\partial t}, \\
&(d)\ \text{displacement current (vacuum)} \\
&\qquad \mathbf{j}_d = \frac{1}{4\pi}\frac{\partial \mathbf{E}}{\partial t}.
\end{aligned}\right\} \tag{29}$$

The ion current, as distinct from the ion-polarization current given above, has been omitted, since it is much smaller in magnitude than the electron current. For the case where the collision frequency is much less than the impressed frequency, the refractive index becomes

$$n = 1 + 2\pi \sum_i \xi_i N_i - \tfrac{1}{2}(\omega_p/\omega)^2 \quad \text{(c.g.s. system)}, \tag{30}$$

where the subscript i refers to ions and atoms.

Fringe shift for argon

When the gas under investigation is traversed over a span of length l by one of the two coherent beams of an interferometer arrangement, a change in its refractivity n is observed as a phase shift, or fringe shift. If λ is the wavelength of the light beam, then a change in optical path $\Delta n \,.\, l$ produces a phase shift of s wavelengths, or

$$\Delta n = \lambda s/l. \tag{31}$$

In what follows, it is convenient to take as reference (subscript 1) the refractive index ahead of the shock front. Then

$$\Delta n = n - n_1, \tag{32}$$

where n is the index in some plane of interest behind the shock front. In applying the fringe shift relation to the experiment, equations (30), (31), and (32) yield the following expression for the fringe shift

$$s = \frac{l}{\lambda}(n_A - 1)_0 \frac{p_1}{p_0}\frac{T_0}{T_1}\left[\left(\frac{\rho}{\rho_1} - 1\right) + \alpha\frac{\rho}{\rho_1}\left\{\frac{\xi_{A^+}}{\xi_A} - 1 - \frac{1}{\xi_A}\left(\frac{q\lambda}{2\pi c\sqrt{m_e}}\right)^2\right\}\right], \tag{33}$$

where $(n_A - 1)_0$ is the reduced refractive index of argon (Edelman & Bright 1948) at standard pressure and temperature (p_0, T_0), and ρ is the mass density at any point behind the shock front. For neutral particles and positive ions, the fringe shift is inversely proportional to the impressed wavelength, but is directly proportional to the wavelength for the electrons. The latter behaviour is due to the dispersive character of the electron refractive index, which is proportional to the square of the impressed wavelength. The electron refractive index is less than unity (phase velocity of the electric field is greater than the speed of light) so that an increase in electron density moves the fringe in a direction opposite to that caused by the heavy gas particles. The estimated basic uncertainty in the measurement of the fringe shift is 0·06 fringes, provided the polarizabilities of the different species are known. Hence, the lowest electron concentration to which the interferometer for present conditions is sensitive is $10^{16}\,\mathrm{cm}^{-3}$, corresponding to about 5 % ionization. As the degree of ionization approaches 15 %, with corresponding electron density of $1{\cdot}9 \times 10^{17}\,\mathrm{cm}^{-3}$, the experimental uncertainty reduces to 5 %.

4. Experimental apparatus and method

The optical properties of the shocked gas were studied with a Mach–Zehnder interferometer by photographing the fringe shift due to changes in the refractive index of the ionized gas. This method has been used to measure polarizability of different atomic species (Alpher & White 1959*a*, Marlow & Bershader 1964), to study relaxation phenomena (Blackman 1956, Byron 1959, Matthews 1959), and to measure electron concentration (Alpher & White 1959*b*, Medford *et al.* 1961, Ramsden & McLean 1962, Shukhtin 1961). The Mach–Zehnder interferometer used was designed by D. Weimer† and was on loan through the courtesy of the Lockheed Palo Alto Research Laboratory. Matched sets of boroscilicate crown-glass optical windows with a $2\frac{3}{4}$ in. diameter, $\frac{3}{4}$ in. thickness, and ground flat to $\frac{1}{4}$ wavelength and parallel to 0·0005 in., were employed.

The studies were performed in an extruded aluminium shock tube‡ 30 ft. in length, with a square interior cross-section (2 in. × 2 in.) and $\frac{3}{4}$ in. wall thickness. The stainless combustion-driver section had an internal diameter of 3 in. and a $1\frac{1}{2}$ in. wall. A combustible mixture of oxygen–hydrogen–helium, using conventional spark ignition, was employed in conjunction with pre-scribed aluminium diaphragms. Two vacuum pumping stations were used to facilitate the evaluation and flushing of the test area. Heating tapes encased the tube and were turned on automatically to aid in outgassing of the system. The test section was designed with a pair of optical windows and with three barium-titanate pressure transducers mounted flush with the interior tube walls, for the purpose of viewing the flow and measuring the shock speed. At the downstream end was a dump tank separated from the test section by a thinly scribed aluminium diaphragm, which broke very rapidly upon the arrival of the shock.

† D. Weimer, Ohio Northern University.

‡ Design of tube was based on plans provided by Professor R. Jahn, California Institute of Technology (now at Princeton University).

To obtain the necessary time resolution to study the relaxation phenomena, two approaches were employed. The first made use of a 3×10^{-7} sec duration spark light source and polaroid film to obtain a 'snapshot' interferogram of the shock flow. This technique encountered problems of blurring and over-exposure caused by the continuum radiation. The second approach was to obtain time-resolved records of interferograms with a rotating mirror camera using Royal X-pan film. A suitable intense light source of 60 μsec duration was provided by an exploding tungsten wire, powered by a $7\frac{1}{2}$ μF condenser charged to 20 kV. The sweep speed of the camera was usually 3 mm/μsec across the film, which gave a time resolution of 0·15 μsec.

To obtain both mass and electron densities from the measurements of the fringe shift, two monochromatic light photographs at different wavelenths were required. This was accomplished by splitting the flow field with two interference filters and recording them simultaneously on the rotating mirror camera. Filters of 4500 Å and 5890 Å with a band width of 90 Å were used and located at the image plane of the test section. Some simultaneous measurements were also made with a photomultiplier and spectrograph (f/12, 90 Å/mm) to record the emitted radiation.

5. Experimental results and discussion

In this section some typical experimental data utilizing the interferometric technique are discussed, and the results reviewed in some detail. The tests were conducted mainly at initial pressures of $p = 3$ mmHg and $p = 5$ mmHg. The Mach numbers ranged from 12 to 18 with corresponding computed electron density as large as 2×10^{17} cm^{-3}. Figures 4 and 5 of plate 1 represent interferograms recorded with a rotating mirror camera. The manner in which the fringes shifted implied that competing ionization processes proceeded at different rates at various distances behind the shock front. At the shock front the fringes were shifted upward, due to the sudden increase in enthalpy, density, and pressure, and the shift was found to agree with predicted values obtained from the shock relations where only the translational modes of the gas were taken into consideration. The initial jump in the fringes at the shock front was larger for shorter wavelength, as the refractive index of the neutral argon was inversely proportional to the wavelength. Upon production of electrons by thermal ionization, the fringes were shifted downward, since they were mainly susceptible to the dispersive nature of the electrons. The appreciable fringe-shift difference between the two wavelengths used, as well as the difference in the fringe width, was apparent. The most striking feature of the fringe profiles for strong shock waves was the rapid downward shift of the fringes, almost similar to another front being produced. Upon reaching a maximum negative shift, the fringe pattern began to slope upward, thereby indicating a loss of electrons by recombination associated with radiation losses. This showed, especially at the highest shock strengths, that the gas did not remain at a constant equilibrium value for any finite length of time. The effect of radiation cooling is under investigation by Wong & Horn (1965). The maximum negative fringe shifts, compared with the values predicted by the Saha equation

based on a more accurate equilibrium constant than given by equation (20), were found to be in good agreement (figure 6). The rotating mirror photographs also showed the sudden appearance of visible emission resulting from free-bound recombination, as was reported by Petschek & Byron (1957).

From the measurements of the fringe shifts at two wavelengths, both density and electron profiles for the non-equilibrium region were deduced (figures 7–10). The three régimes of the proposed model for the mechanism of ionization were then identified. The results for each régime will now be discussed in turn.

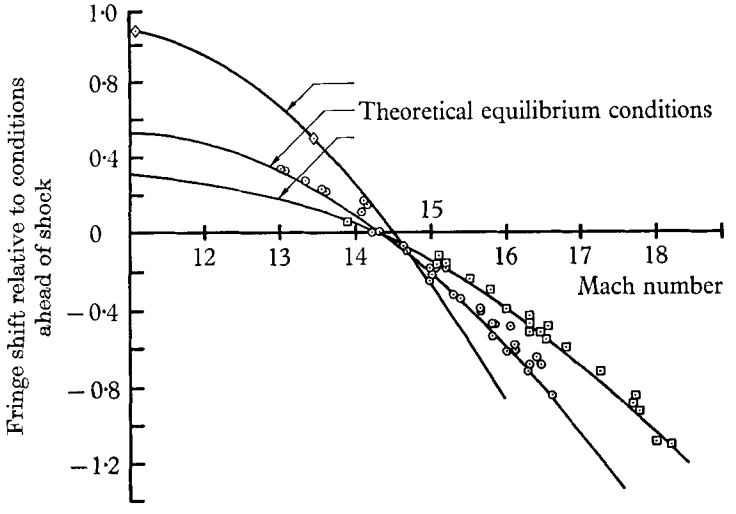

FIGURE 6. Fringe shift at equilibrium conditions for $\lambda = 4500$ Å, $T_1 = 297{\cdot}0$ °K. ◇, $p_1 = 1$ cm; ⊙, $p_1 = 0{\cdot}5$ cm; □, $p_1 = 0{\cdot}3$ cm.

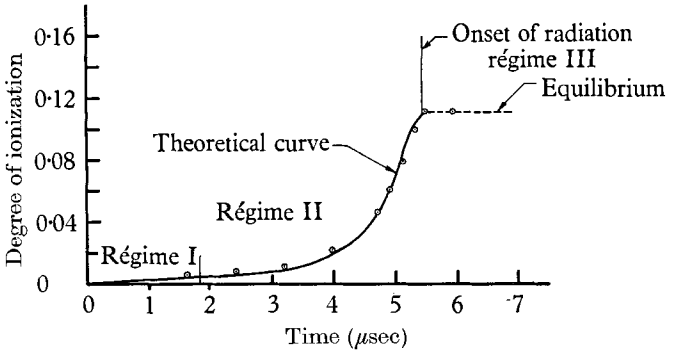

FIGURE 7. Electron-density profile during relaxation for $M = 15$, $p_1 = 0{\cdot}5$ cm. Time (laboratory frame) is measured relative to the shock front.

Régime I

Interferometric techniques at optical wavelengths were insensitive to electrons in régime I ($N_e < 10^{16}$ cm^{-3}). However, in accordance with the discussion in § 2, the inelastic cross-section for atom–atom collisions was obtained by adjusting values to match our overall observed relaxation profiles. This procedure resulted

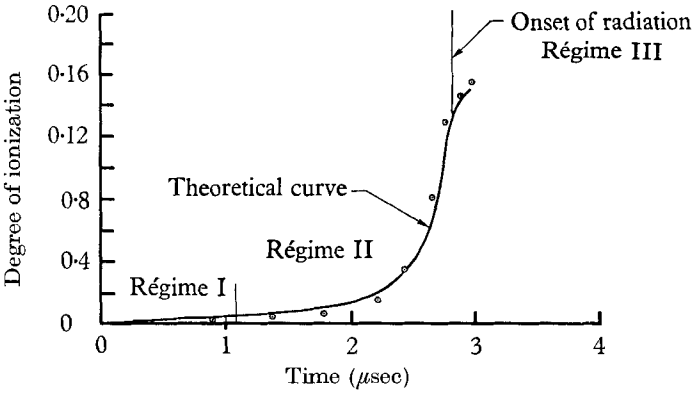

FIGURE 8. Electron-density profile during relaxation for $M = 16{\cdot}3$, $p_1 = 0{\cdot}5$ cm. Time (laboratory frame) is measured relative to the shock front.

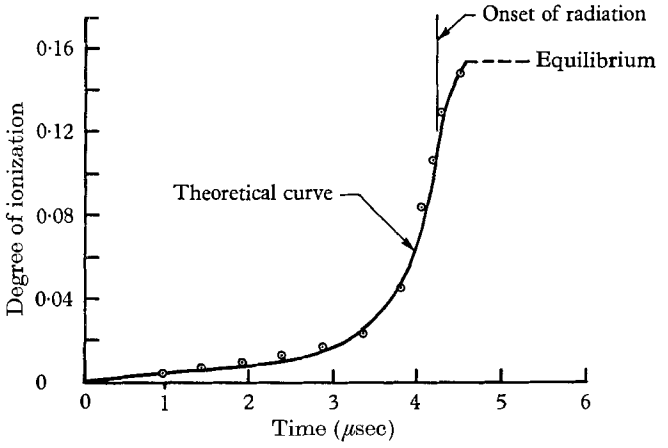

FIGURE 9. Electron-density profile during relaxation for $M = 16{\cdot}3$, $p_1 = 0{\cdot}3$ cm. Time (laboratory frame) is measured relative to the shock front.

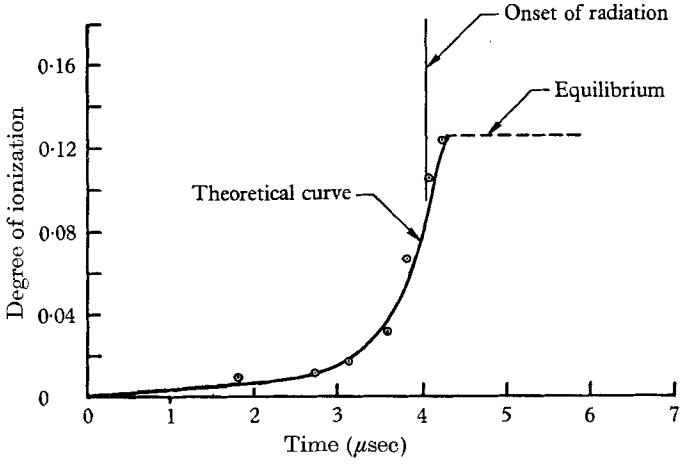

FIGURE 10. Electron-density profile during relaxation for $M = 15{\cdot}4$, $p_1 = 0{\cdot}5$ cm. Time (laboratory frame) is measured relative to the shock front.

in having to reduce the cross-section value reported by Harwell & Jahn (1964) by a factor of 2·5 in order to obtain a compatible value for $K_A(T_A)$ in the equations just mentioned. The value of c_2 in equation (3) as thus adjusted led to the numerical relationship shown between cross-section and energy. However, this relation is expected to be valid only when the gas temperature is low compared with the excitation or ionization temperature, for then the two-step process predominates.

The effects of impurities could never be completely disregarded, even though extreme care was taken to outgas and to flush the system. As we mentioned earlier, the impurity level was reduced to less than 10 parts per million. The influence of impurities was more important at lower initial pressures.

The time-integrated spectrograms of the high-purity tests contained spectral lines with a continuum superimposed upon them. All the spectral lines recorded were identified only as argon. The lack of impurity lines could possibly be due to several factors: to the low intensity of impurity lines, hence negligible amount of impurities; to the relatively large f number (12) of the spectroscope; or to the spectral range of the plates. In any case, this result is at least consistent with our assumption that the effects of impurities had been minimized below a threshold level.

The presence of precursor electrons ahead of the advancing shock front has been reported by many investigators. However, their effect on the relaxation phenomenon has not been studied quantitatively. In our analysis we find that if the precursor-electron concentration reaches a level of $\alpha = 1{\cdot}5 \times 10^{-4}$ at the shock front ($M = 16{\cdot}3$, $p_1 = 0{\cdot}5$ cm Hg), the electron-production mechanism of régime II would become predominating at an earlier stage. As a result both the relaxation period for electron build up in régime I and the total relaxation time may be shortened by 5%. For electron concentration below this level, there is negligible effect.

Régime II

This régime was most accessible to the techniques of optical interferometry. The rapid progress of the electron–atom collision process in electron production was the main element underlying the steep curvature of the fringes here. The cross-section for the process used in our computation of the theoretical curve was approximated from the experimental data given in figure 1. Our formulation should be applicable for electron energies not greater than three times the ionization potential. Outside this range, the cross-section goes through a maximum and begins to decrease (Stubbs *et al.* 1962, and Hagstrum 1953). The point where the ionization mechanism due to electron–atom collisions is equal to that due to atom–atom collisions is plotted for several conditions on figure 11. The cross-over point for electron–atom dominance occurs at a higher degree of ionization for stronger shocks, given the same initial conditions. As the shock is strengthened, the temperature of the atoms and the number of A–A ionizing collisions is increased; thus the time period to reach a certain degree of ionization is shorter. On the other hand, the atom–atom ionization process remains dominant until a larger number of electrons are produced. The factor which governs

the efficiency of the electron–atom process can be clearly seen on figure 12. This graph shows the manner in which electrons acquire energy by colliding elastically with the heavier species. By comparing the curves in figures 11 and 12 at corresponding degrees of ionization, it is apparent that when the electron–atom ionization process becomes dominant, the energy exchange mechanism is primarily one in which electrons gain energy by e–A^+ elastic Coulomb collisions and then utilize it for ionization. This is consistent with the fact that the e–A^+

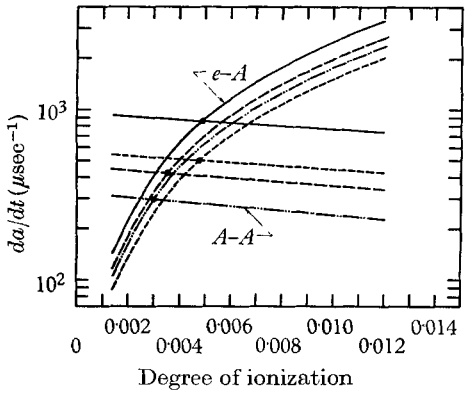

FIGURE 11

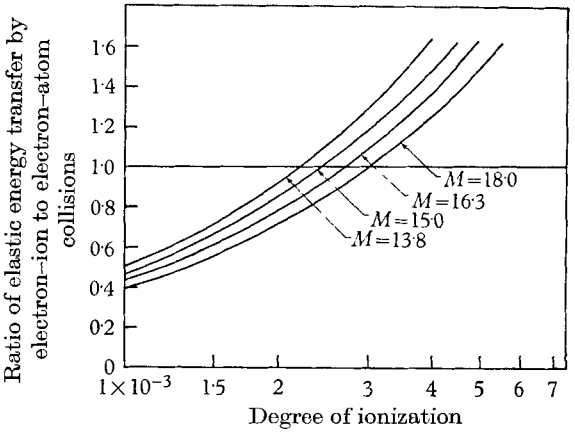

FIGURE 12

FIGURE 11. Comparison of ionization rates between argon–argon and argon–electron collisions. ——, M = 16·3, p_1 = 0·5 cm; — — —, M = 15·4, p_1 = 0·5 cm; — · · —, M = 15·0, p_1 = 0·5 cm; – – –, M = 16·3, p_1 = 0·3 cm.

FIGURE 12. Elastic energy transfer for p_1 = 0·5 cm.

Coulomb cross-section is appreciably larger than the e–A elastic-collision cross-section, especially in the energy range of interest here, where an effect of the Ramsauer minimum (occurring at 0·3 volts) is still felt.

The assumption that the average energy of the electrons did not change appreciably, appeared to be justified. The amount of change which did take place is shown in figure 13. During the early stages of this régime, the electrons did not lose their energy as rapidly as they did during the later stages. As a result, the temperature of the electrons rose slightly to a maximum and then declined as the rate of ionization increased. During this entire period, the atom temperature was seen to fall most abruptly when the electron temperature reached its maximum value. The mass-density profile also increased sharply within the last quarter of the relaxation zone, while the pressure increase was less steep.

Régime III

The onset of visible radiation on the fringe pictures indicated the point where free-bound recombination became important under the constraint of the sensitivity limits of the film itself, and thus marked the inception of régime III. This point appeared to vary both with increase in pressure and shock strength. On the average the degree of ionization at this location corresponded to 82% of the

equilibrium value. If the time interval from the shock front to the plane of radiation onset were taken to be the total relaxation time, the error would not be more than 15%. The theory for recombination as proposed in § 2 could not be verified from present measurements. However, the predicted magnitude for recombination was found not to be greater than the limiting experimental value obtained from the measured electron and mass profiles. Since the ionization-rate constant was found to be much larger than that for recombination throughout the relaxation zone, recombination could be disregarded for the prediction of the profiles (Bond 1957).

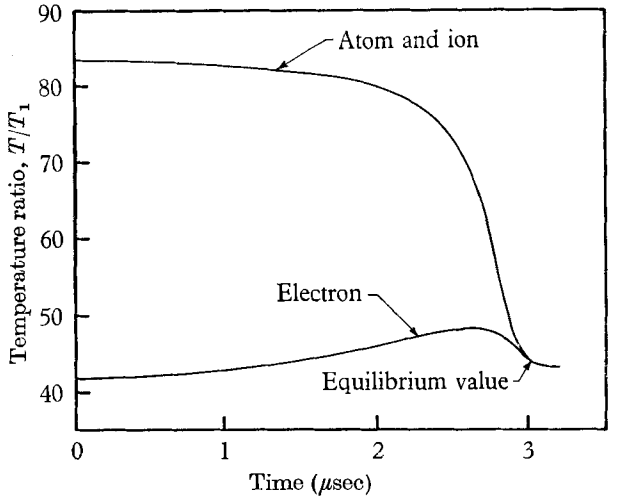

FIGURE 13. Temperature profile during relaxation for $M = 16{\cdot}3$, $p_1 = 0{\cdot}5$ cm, $T_1 = 297$ °K. Time (laboratory frame) is measured relative to the shock front.

The radiation which starts in régime III is seen to persist for a considerable period downstream. The upward sloping fringe pattern, corresponding to a decreasing electron density in an otherwise supposedly uniform régime of gas flow, indicates that appreciable radiation cooling is taking place. This has become the subject of a separate study from which the cooling is found to be largely due to continuum radiation, both free-bound and free-free (Bremstrahlung). The ionization of excited-state atoms could possibly be accomplished by this radiation. Under the present test conditions radiative recombination is small compared with collisional recombination. Thus radiative emission does not appear to play a significant role in the processes leading to thermal ionization equilibration.

Relaxation time

The total ionization relaxation times for various shock strengths are plotted in figure 14. The inverse temperature $1/T_{A0}$, is the temperature behind the shock without ionization. Since the collisional processes for ionization except for recombination are predominantly binary, the relaxation time will exhibit an inverse initial-pressure dependence. Some preliminary experiments ($M > 18$) show that the Saha-equilibrium electron concentration is not reached, and radiation which has been ignored thus far must be included in the analysis.

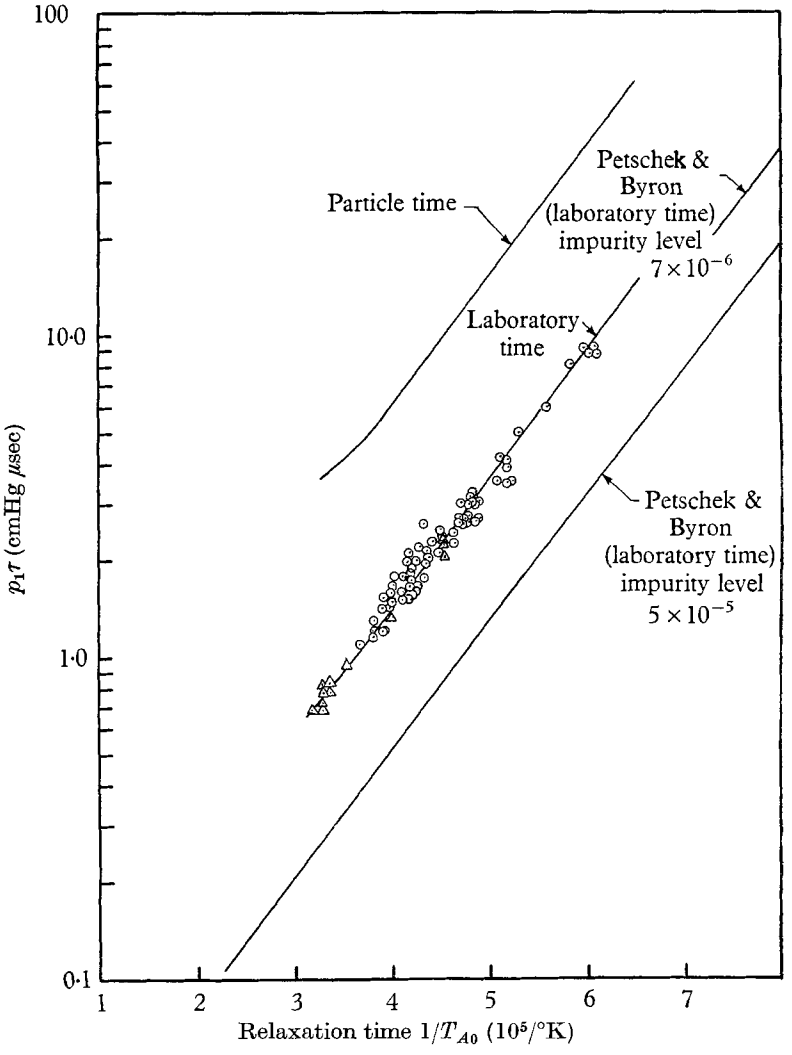

FIGURE 14. Relaxation time as a function of the reciprocal temperature behind the shock with zero ionization. ⊙, $p_1 = 0{\cdot}5$ cm; △, $p_1 = 0{\cdot}3$ cm.

6. Conclusions

The combined results of experiment and theory indicate that the mechanism of ionization can be explained by dividing the relaxation zone into three régimes, each characterized by different dominant collisional processes. Régime I, the early stage of ionization directly behind the shock front, consists primarily of argon atom–atom excitation and ionization collisions. A cross-section for this process was determined, and its dependence on energy near threshold was developed as equation (3). Photo-ionization, precursor effects and impurities do not seem to play a significant role under the tested conditions, until the degree of ionization reaches $1{\cdot}5\times10^{-4}$ at the shock front. Régime II was determined predominantly by electron–atom collisions, and the electrons acquire their energy

for ionization primarily through elastic collisions with the argon ions. Régime III was characterized by the inclusion of recombination in the kinetics of the process. Experimentally, it was marked by the appearance of radiation. However, recombination was found to play a minor role in the determination of the electron profile.

The present study was also concerned with the sensitivity and accuracy of the method of optical interferometry for measuring electron concentration. For electron concentrations greater than $10^{16}\,\mathrm{cm}^{-3}$, the technique is quite acceptable. Good agreement was obtained with equilibrium conditions predicted by the Saha equation, in which the effects of radiation and lowering of the ionization potential were neglected (see figure 6).

We wish to report a stimulating exchange of correspondence with R. A. Alpher of the General Electric Research Laboratory in connection with the present work. This study was supported by the Advance Research Projects Agency of the Department of Defense and The Ford Foundation.

REFERENCES

ALPHER, R. A. & WHITE, D. 1959*a* *Phys. Fluids*, **2**, 153.

ALPHER, R. A. & WHITE, D. 1959*b* *Phys. Fluids*, **2**, 162.

BATES, D. R., KINGSTON, A. E. & MCWHIRTER, R. W. P. 1962 *Proc. Roy. Soc.* A, **267**, 297.

BLACKMAN, V. 1956 *J. Fluid Mech.* **1**, 61.

BOND, J. W. 1957 *Phys. Rev.* **105**, 1683.

BOULEGUE, G., CHANSON, P., COMBE, R., FELIX, M. & STRASMAN, P. 1958 *Proc. 2nd Int. Conf. on Peaceful Uses of Atomic Energy, Geneva*, **31**, 242.

BROWN, E. A. & MULLANEY, J. 1964 *Am. Phys. Soc., Div. Fluid Dyn. Meeting, California.*

BYRON, S. R. 1959 *J. Chem. Phys.* **30**, 1380.

BYRON, S. R., STABLER, R. C. & BORTZ, P. I. 1962 *Phys. Rev. Letters*, **8**, 376.

DE VOTO, R. S. 1964 *Stanford Univ. Dept. of Aero. and Astro. Rep. SUDAER* no. 207.

EDELMAN, G. M. & BRIGHT, M. H. 1948 *MIT Gas Turbine Lab. rep.* no. 6.

HAGSTRUM, D. H. 1953 *Nat. Bureau Standard Circ.* no. 522,193.

HARWELL, K. E. & JAHN, R. G. 1964 *Phys. Fluids*, **7**, 214.

JOHNSTON, N. S. & KORNEGAY, W. 1963 *J. Chem. Phys.* **38**, 2242.

MAIER-LEIBNITZ, V. H. 1935 *Z. Phys.* **95**, 499.

MARLOW, W. C. & BERSHADER, D. 1964 *Phys. Rev.* **133**, A 629.

MATTHEWS, D. L. 1959 *Phys. Fluid*, **2**, 170.

MEDFORD, R. D., POWELL, A. L. T., HUNT, A. G. & WRIGHT, J. K. 1961 *Proc. 5th Int. Conf., Ioniz. Phenom. in Gases, Munich.*

MORGAN, E. J. 1964 *Am. Phys. Soc., Div. Fluid Dyn. Meeting, California.*

PETSCHEK, H. & BYRON, S. R. 1957 *Ann. Phys.* **1**, 270.

RAMSDEN, S. A. & MCLEAN, E. A. 1962 *Nature, Lond.*, **192**, 761.

SHUKHTIN, A. M. 1961 *Optics and Spectroscopy*, **10**, 222.

STUBBS, H. E., DALGARNO, A., LAYZER, D., ASHLEY, E. N., NAQUI, A. & VICTOR, G. 1962 Study of Recombination Phenomena, vol. II. *AFSWC TDR* 62-11.

WEYMANN, H. D. 1958 *Inst. Fluid Dyn. Appl. Math. Univ. of Maryland TN* no. BN-144.

WONG, H. & HORN, K. 1965 *Am. Phys. Soc., 5th Shock Tube Symp. U.S. Naval Ordnance Laboratory, Silver Spring, Maryland.*

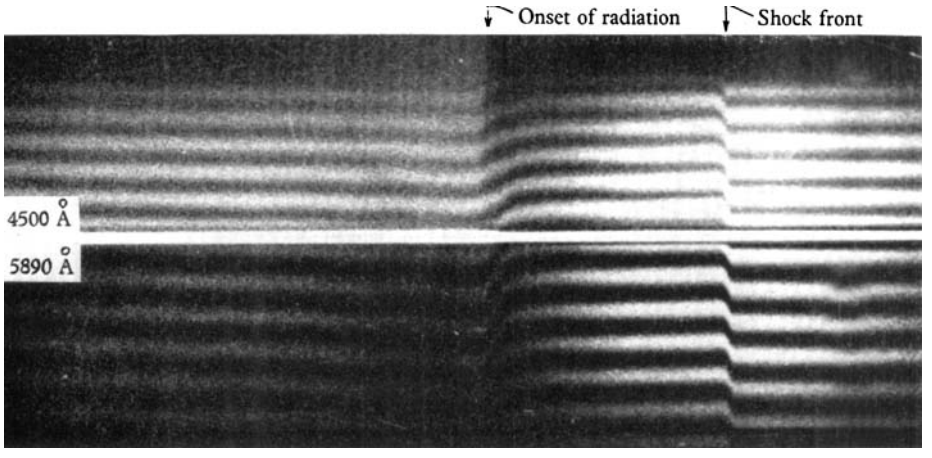

FIGURE 4. Rotating-mirror-camera record of the fringe shift for $M = 15{\cdot}4$, $p_1 = 0{\cdot}5$ cm.

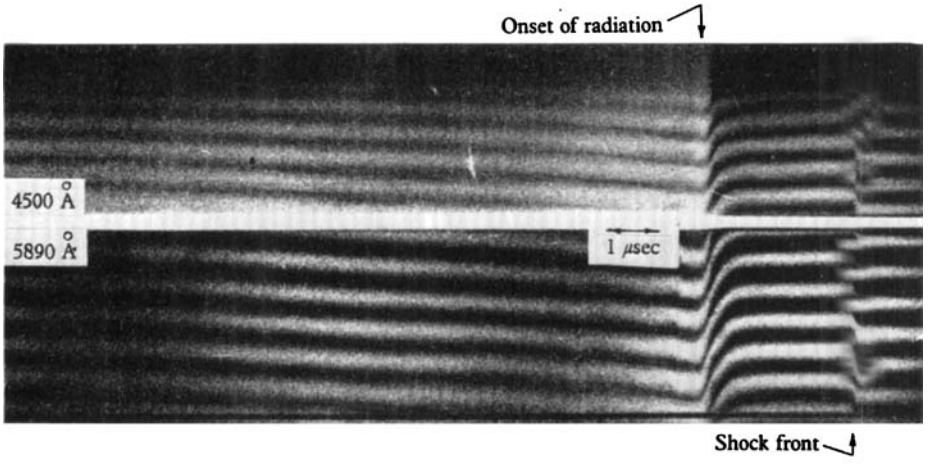

FIGURE 5. Rotating-mirror-camera record of the fringe shift for $M = 16{\cdot}3$, $p_1 = 0{\cdot}5$ cm.